AIAA JOURNAL
Vol. 38, No. 8, August 2000

Approximate Added-Mass Method for Estimating Induced Power for Flapping Flight

S. Sunada* and C. P. Ellington†
University of Cambridge, Cambridge, England CB2 3EJ, United Kingdom

A method that uses the added mass of vortex sheets was developed to estimate induced power in flapping flight for birds and insects. This new method has advantages over existing methods. First, it is valid for flights with any forward velocity. Second, this method can be used to determine the effects of most kinematic parameters of flapping wings on induced power, like the inclination of the stroke plane, amplitude of the flapping angle, and the mean flapping angle. For hovering flight this method has the same accuracy as methods based on the Rankine–Froude momentum theory or on vortex ring theory. When the forward velocity is large, this method agrees with the momentum theory for a fixed wing.

Nomenclature

$(A_{n,m})_k$	= influence matrix
c	= chord length of two-dimensional sheet
d	= vertical distance between vortex sheets
$\hat{f}$	= number of vortex sheets generated during both down and up strokes
g	= gravitational acceleration
h	= height of an isosceles triangle
i, j	= panel number or point number
k	= correction factor or number of a sheet
k_1	$= Mg/\rho R^4 n^2 \Phi^2 \cos^{1.5}\beta$
k_2	$= Mg/\rho R^4 n^2 \Phi^2 \cos^3\beta$
M_A	= added mass of a vortex sheet
$\hat{M}_A$	= nondimensional added mass relative to that of a circular disc, $M_A/(8/3\rho R^3)$
$\bar{M}_A$	= nondimensional added mass of a sheet relative to its area, $M_A/\rho S^{1.5}$
N	= half of number of panels on one sheet
NP	= number of sheets used in calculation
n	= beating frequency, $1/(T_d + T_u)$
n_d	= beating frequency determined by only down stroke, $1/2T_d$
P_i	= induced power
p, q	= parameters for changing horizontal and vertical distances between sheets
R	= wing length
R_{mean}	= mean diameter of a sheet, $\sqrt{(S/\pi)}$
$r1$	= ratio of induced power estimated by the present method when $\hat{f}=1$ and that by method 1, 2, 3, or 4
$r2$	= ratio of induced power estimated by the present method when $\hat{f}=2$ and that by method 1, 2, 3, or 4
S	= area of a sheet
S_m	= area of a panel
T	= thrust
T_d	= period of downstroke
T_u	= period of upstroke
t	= time
V	= forward velocity
w	= induced velocity in far wake
w_{RF}	= induced velocity in near wake by Rankine–Froude momentum theory
w_0	= moving speed of a vortex sheet for calculating added mass
x, y, z	= coordinate systems
β	= inclination of stroke plane
Γ_m	= circulation of the mth vortex ring
ρ	= air density
Φ	= amplitude of flapping angle, $\phi_{\max} - \phi_{\min}$
ϕ	= flapping angle during down stroke, $\bar{\phi} + (\phi/2)\cos[(\pi/T_d)t]$
ϕ_{VP}	= velocity potential

Subscripts and Superscripts

C	= collocation point
max	= maximum value
min	= minimum value
P	= panel
$\bar{\ }$	= mean value

Introduction

Recently, several numerical calculation techniques have been used for analysis of flapping flight. Phlips et al.,[1] Vest and Katz,[2] and Hall and Hall[3] adapted the lifting line theory, the panel method, and the vortex lattice method to flapping flight, respectively, and calculated induced power. These techniques employ fewer assumptions about the wake structure than conventinal methods, which will be discussed later. However, the numerical techniques require considerably more computer power than those methods, and they are still widely used.

One of the conventional methods is by Pennycuick,[4] which is based on momentum theory for a fixed wing and is valid only for fast forward flights. (Hereafter, this method is called method 1.) Another method is by Willmott and Ellington[5] (method 2), which is based on the momentum theory for a rotary wing,[6] and is suitable for hovering flight and forward flight. This method has a correction factor, k in Eq. (11), that depends on the wake geometry. The value of k is normally assumed to be equal to 1.2, but there is little theoretical or experimental evidence to support this.

Yet a third method is from Ellington,[7] which is only for hovering flight (method 3). It uses a steady momentum jet estimate, corrected by a quasi-steady vortex theory for wake periodicity. The fourth method is from Rayner[8–10] (method 4) and is based on vortex ring theory. This method for hovering flight considers the wake evolution from rest,[8] whereas the method for forward flight[9] prescribes the wake geometry. In this model there is thus a gap between the wake model for hovering flight and that for forward flight.

The shortcomings in methods 1–4 are removed in a method newly developed in this paper. In this method induced power is estimated by using the added mass of vortex sheets to estimate the mass flux in the wake. The present method is valid for flights with any forward

Received 23 March 1999; revision received 1 August 1999; accepted for publication 22 November 1999.

*Visiting Researcher, Department of Zoology; currently Senior Researcher, Mechanical Engineering Laboratory, Agency of Industrial Science and Technology, Ministry of International Trade and Industry, 1-2 Namiki, Tsukuba, Ibaraki, 305-8564 Japan; sunada@mel.go.jp.
†Professor of Animal Mechanics, Department of Zoology.

velocity and can estimate the effects of most kinematic variables of flapping wings on induced power, like the inclination of the stroke plane, amplitude of the flapping angle, and the mean flapping angle. Compared with the numerical calculation techniques such as the panel method and the vortex lattice method, the present method requires much less computer power but gives accurate estimates of induced power.

Fluid Dynamic Model

Wake Model

First, we consider a flight where the aerodynamic force providing support to weight is generated by the wings only during the downstroke. In such a flight the wake is shed from the wings only during the downstroke.

The wake behind a wing is represented by vortex sheets (Fig. 1) whose shape in the near wake is the projection of the area swept by the wings on the $x - y$ plane (Fig. 2). This shape is determined by the wing motion and is given by

$$x = R \sin\phi(t)\cos\beta + Vt, \qquad y = R\cos\phi(t) \tag{1}$$

We assume that the variation in flapping angle is sinusoidal:

$$\phi(t) = \bar{\phi} + 0.5\Phi\cos(\pi t / T_d) \qquad (0 \le t \le T_d) \tag{2}$$

In contrast to that in the near wake, the shape of the vortex sheet in the far wake is unknown because of the deformation of the wake.

The induced velocity in the near wake is $0.5w$ and in the far wake is w, similar to those in both the Rankine–Froude momentum theory for a rotary wing[6] and the momentum theory for a fixed wing.[11] The distance in the z direction between two sheets in the near wake and in the far wake is $0.5w/n\hat{f}$ and $w/n\hat{f}$, respectively; and the distance in the x direction between two sheets in the near wake and in the far wake is $V/n\hat{f}$. Here, $\hat{f}$ is a parameter indicating the total number of vortex sheets generated during a wing beat. When

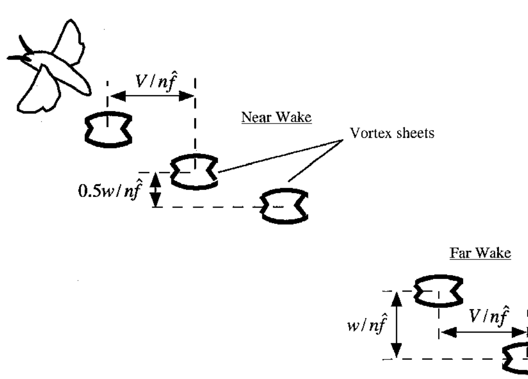

Fig. 1 Wake system.

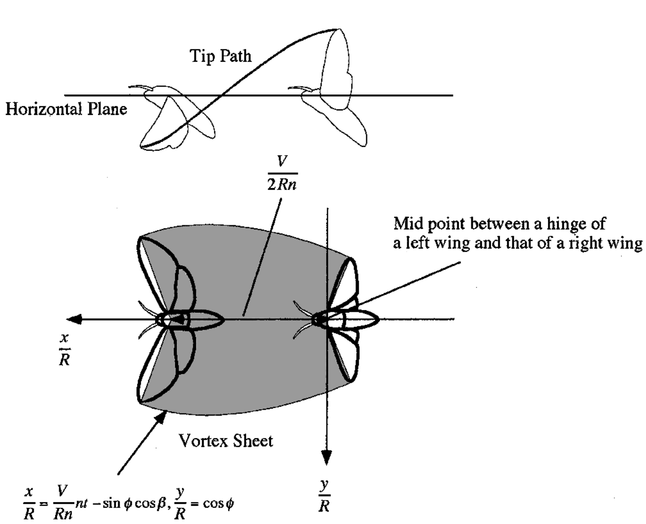

Fig. 2 Shape of a vortex sheet in near wake.

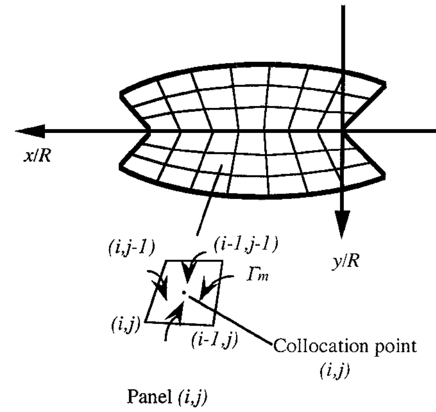

Fig. 3 Vortex ring arrangement on a vortex sheet.

aerodynamic force is generated only during the downstroke, then $\hat{f} = 1$, and during both down- and upstrokes, $\hat{f} = 2$.

The aerodynamic force T and induced power P_i are given by

$$T = M_A w \hat{f} n \tag{3a}$$

$$P_i = 0.5Tw = 0.5M_A w^2 \hat{f} n = 0.5\left(T^2 / M_A \hat{f} n\right) \tag{3b}$$

$$\hat{f} = 1 \tag{3c}$$

where M_A is the added mass of the vortex sheet in the far wake. Because we are considering a flight where aerodynamic force is generated only during the downstroke, $\hat{f} = 1$, as indicated by Eq. (3c).

From the equation of continuity, M_A in the far wake should be equal to that in the near wake. Therefore, in the calculation for the induced power P_i, the M_A in the near wake (Fig. 2) replaces the added mass in the far wake because the shape of the vortex sheet in the far wake is unknown.

The present method is adapted as follows for flights where the vertical aerodynamic force is generated during both the down- and upstrokes: two vortex sheets are generated during the period of $T_d + T_u$. The assumption is made that the shape of the vortex sheet during the upstroke is the same as that during the downstroke. Therefore, Eq. (3c) is replaced by $\hat{f} = 2$.

Calculating the Added Mass of Vortex Sheets[12,13]

The M_A is obtained by numerically solving the flow around vortex sheets (Fig. 2) in the near wake by using the Laplace equation for velocity potential $\nabla^2\phi_{VP} = 0$. The shape of the vortex sheet is given by Eqs. (1) and (2). All sheets are divided into $2N$ small panels, where each panel is represented by a vortex ring whose circulation is $\Gamma_m (1 \le m \le 2N)$, as shown in Fig. 3. Distribution of Γ_m on all vortex sheets is similar. In the present method the value of $2N$ is 1250 because the M_A does not change significantly for $2N \ge 1250$, as indicated in Appendix A. The distribution of panels is symmetric about the x axis, and the condition $\Gamma_m = \Gamma_{2N+1-m}$ is satisfied.

The distance between two sheets in the z direction is $0.5w/n\hat{f}$. Although the number of sheets NP must be theoretically infinite, $NP = 15$ is sufficiently large for the calculations when $w/Rn \ge 0.5$ because M_A does not change significantly for $NP \ge 15$, as stated in Appendix A. The number of sheets NP was 15 for all of the calculations except for those for Fig. 4.

The coordinates of the corners of the (i, j) panel on the kth sheet are expressed as

$$x_P(i, j, k)/R = (j/j_{\max})\sin\phi[t = (i/i_{\max})T_d]\cos\beta + (V/R)[(i/i_{\max})T_d + k/n\hat{f}]$$

$$y_P(i, j, k)/R = (j/j_{\max})\cos\phi[t = (i/i_{\max})T_d]$$

$$z_P(i, j, k)/R = (0.5w/Rn\hat{f})\{k - [(NP + 1)/2]\} \tag{4}$$

Collocation points are at the center of the vortex rings only on the middle sheet, $k = (NP + 1)/2$. The coordinates of the collocation points are

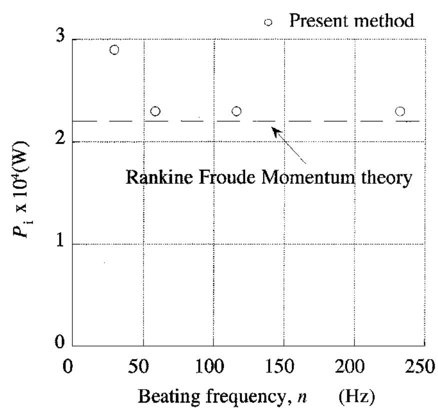

Fig. 4 Comparison between the present method and the Rankine–Froude momentum theory for calculating the induced power for various beating frequency n.

$$x_C(i, j) = [x_P(i-1, j-1) + x_P(i-1, j) + x_P(i, j-1) + x_P(i, j)]/4$$

$$y_C(i, j) = [y_P(i-1, j-1) + y_P(i-1, j) + y_P(i, j-1) + x_P(i, j)]/4$$

$$z_C(i, j) = 0 \tag{5}$$

Here is considered an imaginary motion where all sheets move in the z direction with velocity w_0. The following condition must be satisfied at all collocation points:

$$\sum_{k=1}^{NP} (A_{n,m})_k \begin{bmatrix} \Gamma_1 \\ \cdots \\ \Gamma_m \\ \cdots \\ \Gamma_N \end{bmatrix} + w_0 \begin{bmatrix} 1 \\ \cdots \\ 1 \\ \cdots \\ 1 \end{bmatrix} = \begin{bmatrix} 0 \\ \cdots \\ 0 \\ \cdots \\ 0 \end{bmatrix} \tag{6}$$

where $(A_{n,m})_k$ is an influence matrix that indicates the influence of both mth and $(2N+1-m)$th vortex rings on the kth sheet for the nth collocation point. The circulation $\Gamma_m (1 \leq m \leq N)$ is determined by solving Eq. (6). Then, M_A is given by

$$M_A = 2\rho \sum_{m=1}^{N} S_m \frac{\Gamma_m}{w_0} \tag{7}$$

where S_m is the area of the mth vortex ring. The following relation between the interference effect between vortex sheets on the added mass can be expected from Eqs. (6) and (7). When the distance between vortex sheets is smaller, that is, when the interference effect between the vortex sheets is larger, the coefficients in influence matrix $(A_{n,m})_k$ become larger, and the added mass determined by the obtained circulation and Eq. (7) is smaller. Thus, the interference effect between vortex sheets makes the added mass of the vortex sheets smaller.

Results

Numerical Error in the Present Method

Figure 5 shows $\hat{M}_A = M_A/(8/3\rho R^3)$ for an isolated sheet; this is the nondimensional added mass relative to that of a circular disc, $8/3\rho R^3$. In this figure $\phi_{max} = -\phi_{min} = 0.5\Phi$ and $V = 0$. The values of $\hat{M}_A$ are a function of β and Φ. For $\Phi = 180$ deg, the shape of the sheet is circular for $\beta = 0$ and elliptic for other values of β. The cross symbols in the figure show the values of $\hat{M}_A$ for $\Phi = 180$ deg calculated by the present method, and the solid line shows the corresponding analytical values of $\hat{M}_A$ (Ref. 14). The difference between the calculated and the analytical values was less than 5%. The other symbols and lines in the figure will be used later for the definition of k_1.

We determined the error in the present method for a series of sheets by calculating M_A for stacked two-dimensional sheets, and

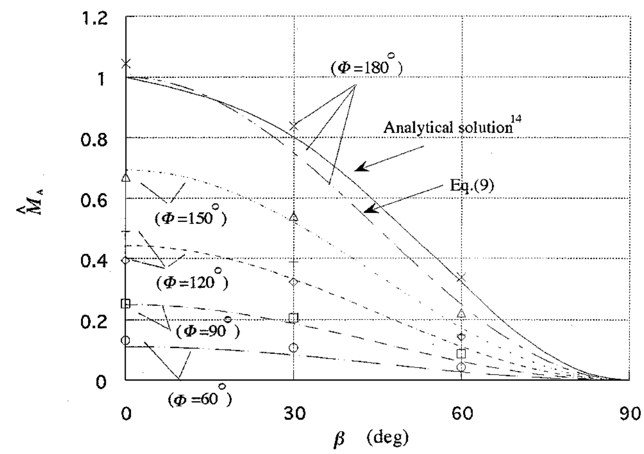

Fig. 5 Effect of inclination of stroke plane β and amplitude of flapping angle Φ on added mass. Symbols show the values calculated by the present method: ——, analytical value at $\Phi = 180$ deg. The other lines indicate the values calculated by Eq. (9) at various Φ.

then comparing these values of M_A with the analytical solution calculated using the following equation[15]:

$$\frac{M_A}{M_A(d/c = \infty)} = \frac{8}{\pi^2}\left(\frac{d}{c}\right)^2 \ln\left\{\cosh\left(\frac{\pi c}{2d}\right)\right\}$$

$$M_A(d/c = \infty) = \frac{\pi}{4}\rho c^2 \tag{8}$$

The present method overestimated the value of M_A of the stacked two-dimensional sheet by about 5%. This means that the estimated error in the present method is less than 5%.

Comparison of Methods

The present method, with $\beta = \phi_{max} = \phi_{min} = n = n_d = 0$, agrees with the momentum theory for a fixed wing because the vortex system is the same in both.

Figure 4 shows values of P_i calculated by using the present method as a function of beating frequency n. For the calculation the following kinematics data were used: $\beta = 0$ deg, $V = 0$, $\phi_{max} = -\phi_{min} = 90$ deg, $R = 17.4$ mm, and $M = 0.0498$ g. Here, wing length R and the total mass M are those for the cranefly (Appendix B). In these calculations the number of the sheets NP is much larger than $NP = 15$, which was for the other calculations in this paper, as stated in Appendix A.

The calculated P_i approaches that based on the Rankine–Froude momentum theory when n becomes larger. This can be explained by considering the wake model in the Rankine–Froude momentum theory as follows. An actuator disk, representing an infinite number of blades, is assumed in the Rankine–Froude momentum theory. Vortices are steadily generated from the rotating blades and exist everywhere in the vortex tube, which represents the wake under the actuator disk. So, the vortex tube is equivalent to a stack of vortex sheets the distance between which is zero. In the present method vortex sheets are generated almost continuously as n approaches infinity. Therefore the wake model in the present method as n approaches infinity agrees with that in the Rankine–Froude momentum theory. Conversely, when n is small, the difference between the wake model in the present method and that in the Rankine–Froude momentum theory is larger, and the difference between the P_i is larger.

The preceding reasoning is valid in general, and not just for the specific example of the cranefly in Fig. 4. Therefore, the present method is consistent with both the momentum theory for a fixed wing and the Rankine–Froude momentum theory for a rotary wing.

Parameters k_1 and k_2

A parameter k_1 is useful for estimating the interference effect between vortex sheets in the present method and a parameter k_2 for estimating the correction factor k in Eq. (13).

Table 1 Parameters indicating interference effect between vortex sheets in hovering flight[7,16,17]

Insect	Body mass mg	Wing length R, mm	Beating frequency n, Hz	Inclination of stroke plane β, deg	Amplitude of flapping angle Φ, rad/deg	$k_1 = \dfrac{Mg}{\rho R^4 n^2 \Phi^2 \cos^{1.5}\beta}$	$k_2 = \dfrac{Mg}{\rho R^4 n^2 \Phi^2 \cos^3\beta}$
Ladybird, Coccinella 7-punctata	34.4	11.2	53.9	18	3.09/177	0.68	0.73
Cranefly, Tipula obsoleta	11.4	12.7	45.5	11	2.13/122	0.38	0.39
Cranefly, Tipula paludosa[a]	49.8	17.4	58.0	6	2.09/120	0.30	0.30
Honeybee, Apis mellifera	101.9	9.8	197	−11	2.27/130	0.45	0.47
Hoverfly, Eristalis tenax	68.4	11.4	157	0	1.90/109	0.36	0.36
Hoverfly, Episyrphus balteatus	27.3	9.3	159	−2	1.66/95	0.42	0.42
Hoverfly, Episyrphus balteatus	28.1	10.0	141	21	1.15/66	0.95	1.05
Hawkmoth, Manduca sexta[a]	1995	52.1	25.4	23.4	1.97/113.1	0.98	1.11
Bumblebee, Bombus terrestris[a]	175	13.2	155	6	2.02/116.0	0.47	0.48
Bumblebee, Bombus hortorum	226	14.1	152	−8	2.09/120	0.46	0.47
Bumblebee, Bombus lucorum	231	14.1	140	6	2.27/130	0.47	0.47

[a]Cases calculated.

Table 2 Comparison of the five methods of induced power of cranefly flight

Present method		Method 1		Method 2 (k = 1.2)		Method 3		Method 4		
		P_i	$r1$ or $r2$	P_i	$r1$ or $r2$	P_i	$r1$ or $r2$		P_i	$r1$ or $r2$
				V/Rn = 0						
$\hat{f}$ = 2	3.1×10^{-4}W			3.3×10^{-4}W	$r2$ = 1.06	3.1×10^{-4}W	$r2$ = 1.0	Normal hovering		
								$S = \Phi R^2$	3.5×10^{-4}W	$r2$ = 1.13
$\hat{f}$ = 1	3.8×10^{-4}W				$r1$ = 0.87		$r1$ = 0.82	$S = \pi R^2$	2.8×10^{-4}W	$r2$ = 0.90
								Avian hovering		
								$S = \Phi R^2$	3.9×10^{-4}W	$r1$ = 1.03
								$S = \pi R^2$	3.2×10^{-4}W	$r1$ = 0.84
				V/Rn = 0.376						
$\hat{f}$ = 2	2.6×10^{-4}W	3.3×10^{-4}W	$r2$ = 1.27	3.0×10^{-4}W	$r2$ = 1.15					
$\hat{f}$ = 1	3.2×10^{-4}W		$r1$ = 1.03		$r1$ = 0.94					

Parameter k_1: Indicator of Interference Effect Between Wake Sheets During Hovering Flight

The symbols in Fig. 5 indicate the added mass $\hat{M}_A$ of isolated sheets calculated using the present method when $V = 0$ as parameters of β, $\phi_{\max}$, and $\phi_{\min}$. The solid line shows the analytical solution at $\phi_{\max} = -\phi_{\min} = 90$ deg, and the other five lines indicate $\hat{M}_A$ calculated using the equation

$$\hat{M}_A = \cos^{1.5}\beta(\Phi/180\,\mathrm{deg})^2 \tag{9}$$

The calculated values of $\hat{M}_A$ by the present numerical method (symbols) are similar to those from Eq. (9). Substituting Eq. (9) and $T = Mg$ into Eq. (3a) yields a nondimensional distance between sheets $w/R\hat{f}n$ that is proportional to k_1, which is a parameter that indicates the magnitude of the interference effect:

$$w/R\hat{f}n \propto Mg/\rho R^4 n^2 \Phi^2 \cos^{1.5}\beta \equiv k_1 \tag{10}$$

Parameter k_2: Indicator of Correction Factor k

In the momentum theory modified for a beating wing by Willmott and Ellington,[5] induced velocity in the far wake w is given by

$$w = 2\sqrt{-\tfrac{1}{2}V^2 + \sqrt{(kw_{\mathrm{RF}})^4 + 0.25V^4}}$$
$$w_{\mathrm{RF}} = \sqrt{Mg/2\rho\Phi R^2} \tag{11}$$

The value of k is normally taken as 1.2, but it should vary according to the wing kinematics, and the validity of the assumption that $k = 1.2$ is not yet known.

When the induced velocity w calculated using Eq. (11) is equal to that using the present method, the correction factor k is given by

$$k = \frac{3}{8\hat{M}_A}\sqrt{\frac{1}{2}\frac{g}{\rho}\frac{M}{R^4\hat{f}^2n^2}\Phi} \times \sqrt[4]{1 + \left(\frac{16\rho}{3g}\right)^2\left(\frac{R^4\hat{f}^2n^2}{M}\right)^2\left(\frac{V}{Rn}\right)^2\hat{M}_A^2} \tag{12}$$

For hovering flight this factor is

$$k = \frac{3}{8\hat{M}_A}\sqrt{\frac{1}{2}\frac{g}{\rho}\frac{M}{R^4\hat{f}^2n^2}\Phi} \propto \frac{Mg}{\rho R^4 n^2 \Phi^2 \cos^3\beta} \equiv k_2 \tag{13}$$

The value of k_2 is therefore proportional to the correction factor k.

The values of k_1 and k_2 are similar; indeed, $k_2 = k_1/\cos^{1.5}\beta$. When the interference effect (i.e., $1/k_1$) is small, then k_2 and k are large, and conversely k is small when the interference effect is large.

Table 1 shows values of k_1 and k_2 for some insects.[7,16,17] The smallest interference effect and the largest k occurred for the hawkmoth during hovering flight because of the values of k_1 and k_2, respectively. Conversely, the largest interference effect and the smallest k occurred for the cranefly during hovering flight.

Induced Power for Real Flights

The effectiveness of the present method was determined by calculating P_i for the flights of a cranefly, pigeon, hawkmoth, and bumblebee. The shape of the vortex sheets were determined by using kinematic data for a cranefly,[7] pigeon,[4] hawkmoth,[16] and bumblebee[17] shown in Table B1. Calculations for the flights were made under two assumptions. First, the vertical force is generated during only the downstroke, which is generally true for forward flight. Second, it is generated during both strokes, which applies to most hovering insects and hummingbirds.

The correction factors k for the different flights are shown in Fig. 6. The assumption of $k = 1.2$ gives a good estimate of induced power for forward flight, where $\hat{f} = 1$. However, the value of k is 2.2 for the hovering flight of a hawkmoth, where the aerodynamic force is generated during only the downstroke, the assumption that $k = 1.2$ would cause a large error in estimating the induced velocity by Eq. (11).

The P_i for a cranefly flight for a forward velocity V/Rn of 0 and 0.376 (Table 2) was calculated by using five different methods: the present method and methods 1–4. Vertical body velocity was

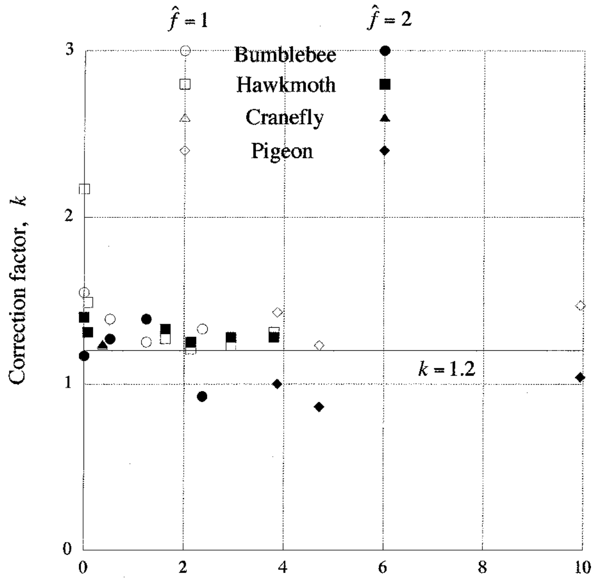

Fig. 6 Correction factor k for flights of a bumblebee, a hawkmoth, a cranefly, and a pigeon. Kinematic data are shown in Table B1. Calculations done for $\hat{f} = 1$ and 2.

neglected in all methods. The calculations using the present method were made under both cases and $\hat{f} = 1$ and 2.

Table 2 shows the comparison between the present method and methods 2–4 for $V/Rn = 0$. The result from the present method with $\hat{f} = 2$ agrees very well with that from method 2 ($r2 = 1.06$) and method 3 ($r2 = 1.0$). This result also agrees with that by method 4 for normal hovering, which is equivalent to $\hat{f} = 2$ ($r2 = 1.13$ when $S = \Phi R^2$ or $r2 = 0.9$ when $S = \pi R^2$). In addition, the result from the present method with $\hat{f} = 1$ agrees reasonably well with that from method 2 ($r1 = 0.87$), method 3 ($r1 = 0.82$), and method 4 for avian hovering, equivalent to $\hat{f} = 1$ ($r1 = 1.03$ when $S = \Phi R^2$ or $r1 = 0.84$ when $S = \pi R^2$). The differences in the estimated induced power of the cranefly flight between the present method and methods 2, 3, and 4 are small when $V/Rn = 0$.

Table 2 also shows the comparison between the present method and methods 1 and 2 for slow forward flight at $V/Rn = 0.376$. The result from the present method with $\hat{f} = 2$ agrees reasonably well with that from method 2 ($r2 = 1.15$). There is a larger difference between the present method with $\hat{f} = 2$ and method 1 ($r2 = 1.27$), but that method is based on the momentum theory for fast forward flight, as stated before; it is not suitable for small forward velocities such as $V/Rn = 0$ or 0.376.

The values estimated by the present method with $\hat{f} = 1$ agree well with those by method 1 ($r1 = 1.03$) and method 2 ($r1 = 0.94$). So, methods 1 and 2 with $k = 1.2$ can estimate induced power as precisely as the present method for flight with small V/Rn when aerodynamic force is generated only during the downstroke.

Among the flights listed in Table B1, the cranefly has the smallest k_1, i.e., the smallest nondimensional distance between vortex sheets ($= d/2R$), and the largest k_2, i.e., the largest interference effect between vortex sheets. When the aerodynamic force was assumed to be generated 1) during the downstroke ($\hat{f} = 1$), the interference effect decreased the added mass of the vortex sheet by 35%, and $d/2R = 0.5(w/R\hat{f}n)$ was 0.76, and 2) during both strokes ($\hat{f} = 2$), 41% and 0.3, respectively. This means that for other flights the expected $d/2R$ is greater than 0.3.

Interference Effect Between the Vortex Sheets on Added Mass

Added mass was estimated for a series of circular sheets (Fig. 7a) for various horizontal and vertical distances (pR and qR, respectively) between vortex sheets. The added mass is nondimensionalized by that of an isolated circular plate $M_A(p = q = \infty)$. At $p \leq 1.5$ (Fig. 7b), $M_A/M_A(p, q = \infty)$ was less than one and increased when q increased. Conversely, at $p \geq 1.5$, M_A/M_A $(p, q = \infty)$ increased

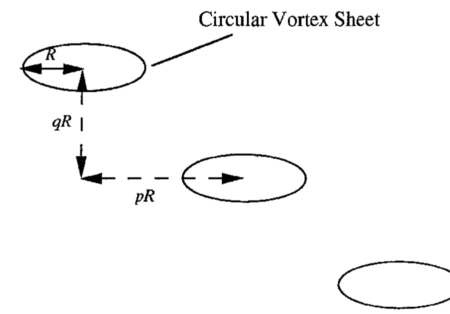

a) Horizontal and vertical distances between circular sheets pR and qR

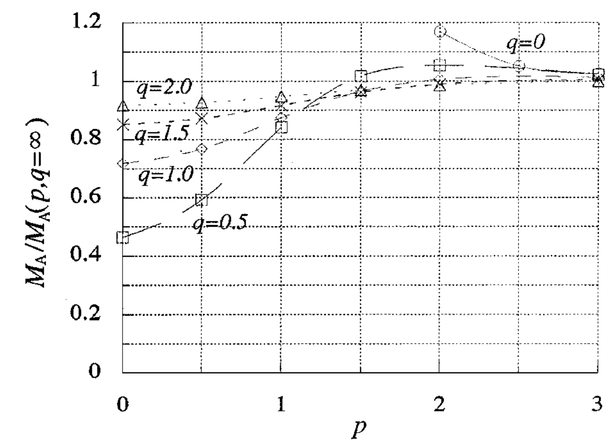

b) Added masses as a function of p and q

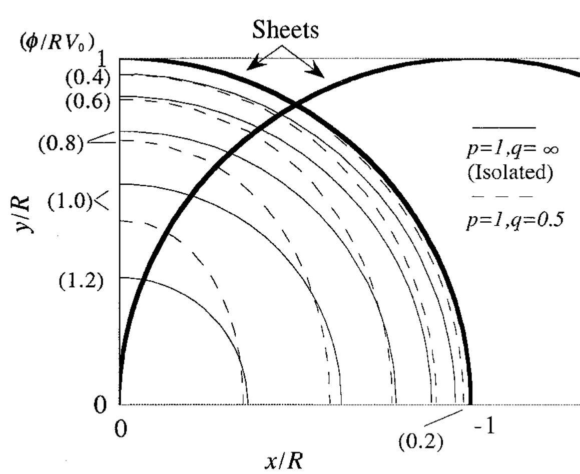

c) Circulation contours for $p = 1$, $q = 0.5$ and $p = 1$, $q = \infty$

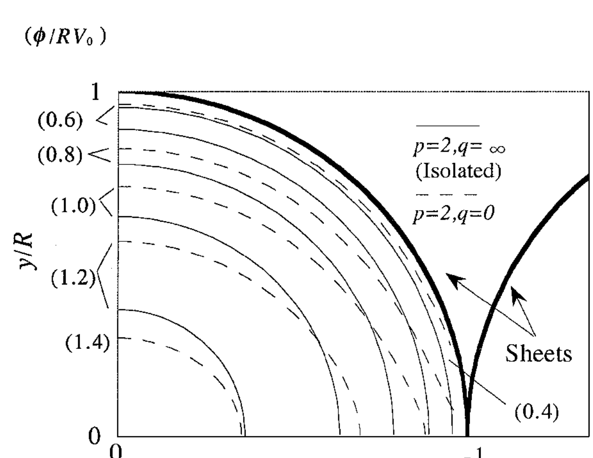

d) Circulation contours for $p = 2$, $q = 0.5$ and $p = 2$, $q = \infty$

Fig. 7 Added mass of series of circular sheets.

when q decreased, and $M_A/M_A(p, q=\infty)$ exceeded one. The reason for these results is that at $p \geq 1.5$ much of each sheet is in the upwash generated by the other sheets, whereas at $p \leq 1.5$ it is in the downwash. Figures 7c and 7d show the interference effect on circulation distribution at $p=1$, $q=0.5$, and $p=2$, $q=0$, respectively. At $p=1$, $q=0.5$ the circulation at any point on the sheet decreased because of the interference effect (Fig. 7c). The decrease in the region where the sheets overlapped in the z direction was particularly large because the downwash generated by the other sheets was larger in this region. At $p=2$, $q=0$ the circulation at any point on the sheet increased because of the interference effect (Fig. 7d). The increase in the region closer to the neighboring sheets was larger because the upwash generated by the other sheets was larger in this region.

The interference effect was largest at $q=0$ when sheets did not overlap each other in the z direction (i.e., at $p \geq 2$), and $M_A/M_A(p, q=\infty)$ did not exceed 1.2. Therefore, the interference effect is not very large when sheets do not overlap each other in the z direction.

For the interference effect between sheets stacked in the z direction ($V/Rn=0$, i.e., $p=0$), the results for six different sheets are shown in Fig. 8, when d/c or $d/2R$ exceeds 0.3, because the expected value for d/c or $d/2R$ is greater than 0.3 as described in the preceding section. The parameters for the six sheets in Fig. 8 are as follows: 1) two-dimensional sheet with chord length c ($R_{\text{mean}}/R=1$) (solid line); 2) circular sheet, $\phi_{\max}=-\phi_{\min}=90$ deg, $\beta=0$ deg, $R_{\text{mean}}/R=1$ (circles); 3) one section of a circular sheet, $\phi_{\max}=-\phi_{\min}=60$ deg, $\beta=0$ deg, $R_{\text{mean}}/R=0.82$ (crosses); 4) one section of a circular sheet, $\phi_{\max}=-\phi_{\min}=30$ deg, $\beta=0$ deg, $R_{\text{mean}}/R=0.58$ (triangles); 5) elliptical sheet, $\phi_{\max}=-\phi_{\min}=90$ deg, $\beta=30$ deg, $R_{\text{mean}}/R=0.93$ (squares); and 6) elliptical sheet, $\phi_{\max}=-\phi_{\min}=90$ deg, $\beta=60$ deg, $R_{\text{mean}}/R=0.71$ (diamonds).

Here, $R_{\text{mean}}[=\sqrt{(S/\pi)}]$ is the diameter of a circle whose area is equal to that of the sheet. The interference effect increased as R_{mean}/R was decreased.

Wing Motion for Smaller Induced Power

Equation (3b) indicates that P_i decreases as M_A increases, when R, n, and $\hat{f}$ are fixed. The relation between w/Rn and $M_A/M_A(w/Rn=\infty)$ and was similar for all three-dimensional vortex sheets in Fig. 8 and is therefore independent of the vortex sheet shape. Therefore, when $M_A(w/Rn=\infty)$ of a vortex sheet shape is large, $M_A=[M_A/M_A(w/Rn=\infty)]\,M_A(w/Rn=\infty)$ is also large, and P_i is small.

The values of M_A of an isolated sheet are calculated for different parameters of wing motions (Table 3). Figure 9 shows $\hat{M}_A=M_A/(8/3\rho R^3)$ for $\beta=0$, 30, 60, and 90 deg.

Optimal wing kinematics for birds and insects might be those that generate the smallest P_i. To decrease P_i, $\hat{M}_A$ must be increased. For

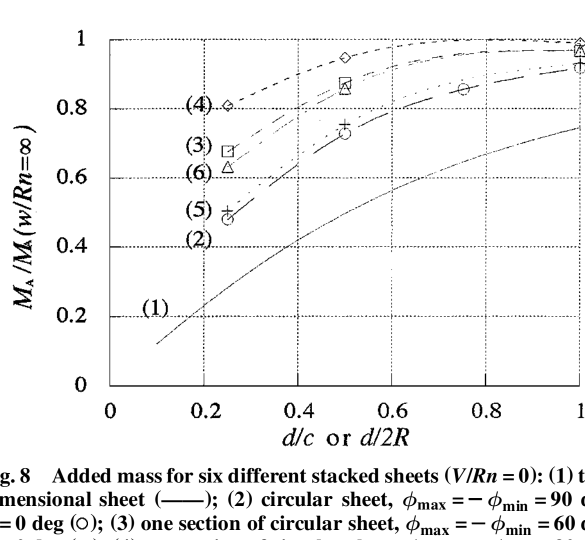

Fig. 8 Added mass for six different stacked sheets ($V/Rn=0$): (1) two-dimensional sheet (——); (2) circular sheet, $\phi_{\max}=-\phi_{\min}=90$ deg, $\beta=0$ deg (○); (3) one section of circular sheet, $\phi_{\max}=-\phi_{\min}=60$ deg, $\beta=0$ deg (□); (4) one section of circular sheet, $\phi_{\max}=-\phi_{\min}=30$ deg, $\beta=0$ deg (◇); (5) elliptical sheet, $\phi_{\max}=-\phi_{\min}=90$ deg, $\beta=60$ deg (+); and (6) elliptical sheet, $\phi_{\max}=-\phi_{\min}=90$ deg, $\beta=30$ deg (△).

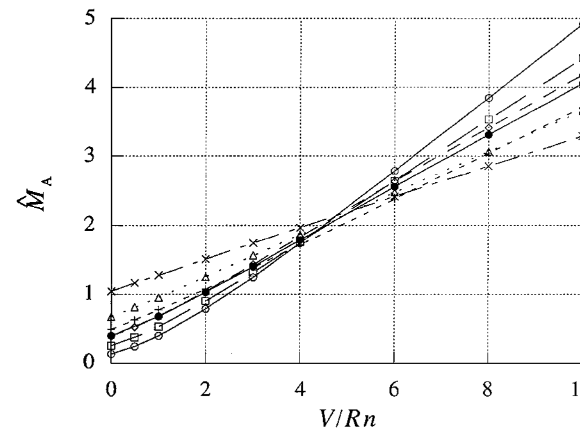

a) $\beta=0$

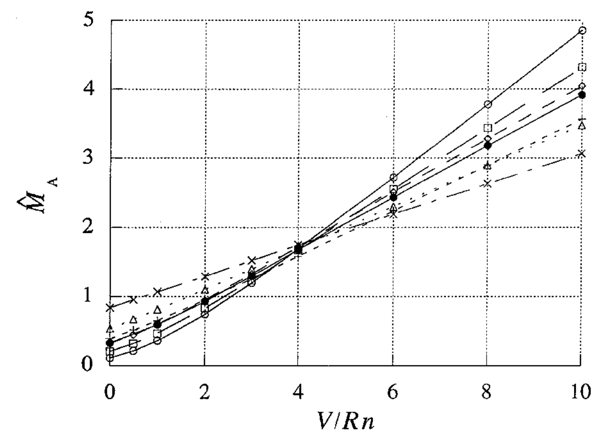

b) $\beta=30$ (deg)

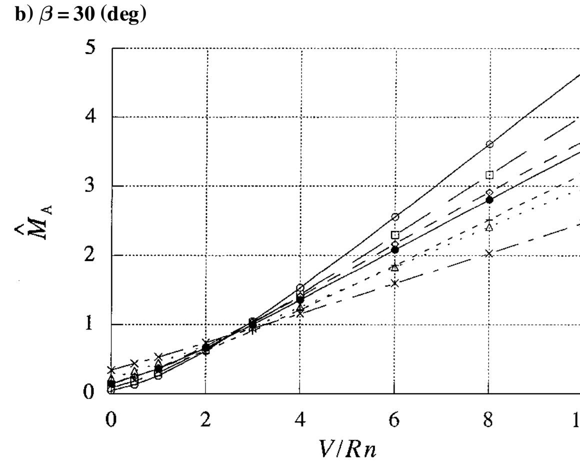

c) $\beta=60$ (deg)

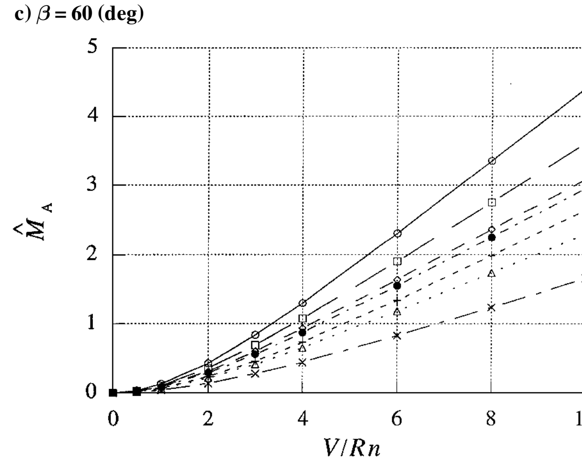

d) $\beta=90$ (deg)

Fig. 9 Nondimensional added mass $\hat{M}_A$ of an isolated sheet. ($\phi_{\max}$, $\phi_{\min}$): ○, (30,−30); □, (60,−30); ◇, (60,−60); ●, (75,−45); +, (90,−30); △ (90,−60); and ×, (90,−90).

Table 3 Cases calculated

V/Rn	β, deg	(ϕ_{max}, ϕ_{min}), deg
0.0	0	(30, −30)
0.5	30	(60, −30)
1.0	60	(60, −60)
2.0	90	(75, −45)
3.0	——	(90, −30)
4.0	——	(90, −60)
——	——	(90, −90)

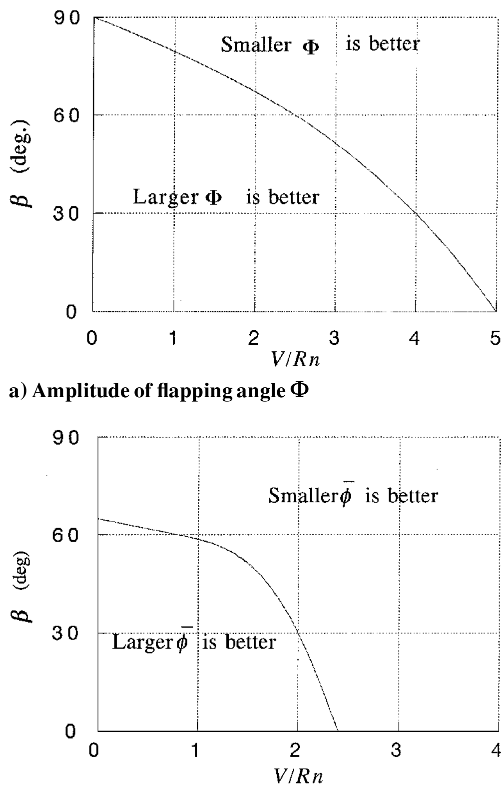

a) Amplitude of flapping angle Φ

b) Mean flapping angle $\bar{\phi}$

Fig. 10 Effect of wing kinematic data on added mass of a vortex sheet.

such conditions Fig. 10 shows the optimal Φ and $\bar{\phi}$ for a given $\bar{\phi}$ and Φ, respectively, as functions of β and V/Rn. Figure 10a shows that a larger Φ is optimal when both V/Rn and β are small. Conversely, a smaller Φ is optimal when both V/Rn and β are large. These results agree with real flights: the flapping amplitude Φ is small for a flyer whose flight is generally fast with large β, and, conversely, Φ is large for a flyer whose flight is generally slow with small β.

Typically, the amplitude Φ is often about 120 deg, but the mean flapping angle can range from 30 to 0 deg. The results in Fig. 10b show the comparison between $\hat{M}_A$ for these conditions. For smaller P_i a larger $\bar{\phi}$ is optimal when both V/Rn and β are small. Conversely, a smaller $\bar{\phi}$ is optimal when either V/Rn or β is large. These results are concurrent with real flight: $\bar{\phi}$ is small for a flyer whose flight is generally fast with large β, and a flyer whose flight is generally slow with small β sometimes uses the clap-fling mechanism, where ϕ_{max} is equal to 90 deg and $\bar{\phi}$ is greater than 0.

$\hat{M}_A$ is determined not only by the shape of the vortex sheet but also the areas of the sheet. It is therefore convenient to define a nondimensional added mass $\bar{M}_A = M_A/\rho S^{1.5}$ (Fig. 11). The $\bar{M}_A$ increases as the shape of the sheet approaches that of a square or circle (see Appendix C). The variations in $\hat{M}_A$ include those for $\bar{M}_A$ and those for the vortex-sheet area.

At $V/Rn \geq 2$

The value of $\bar{M}_A$ declines from about 0.45 to 0.4 and is largely independent of ϕ_{max}, ϕ_{min}, and β because variations in these parameters do not significantly affect the vortex-sheet shape. The variation in $\hat{M}_A$ is mainly caused only by changes in the vortex-sheet area.

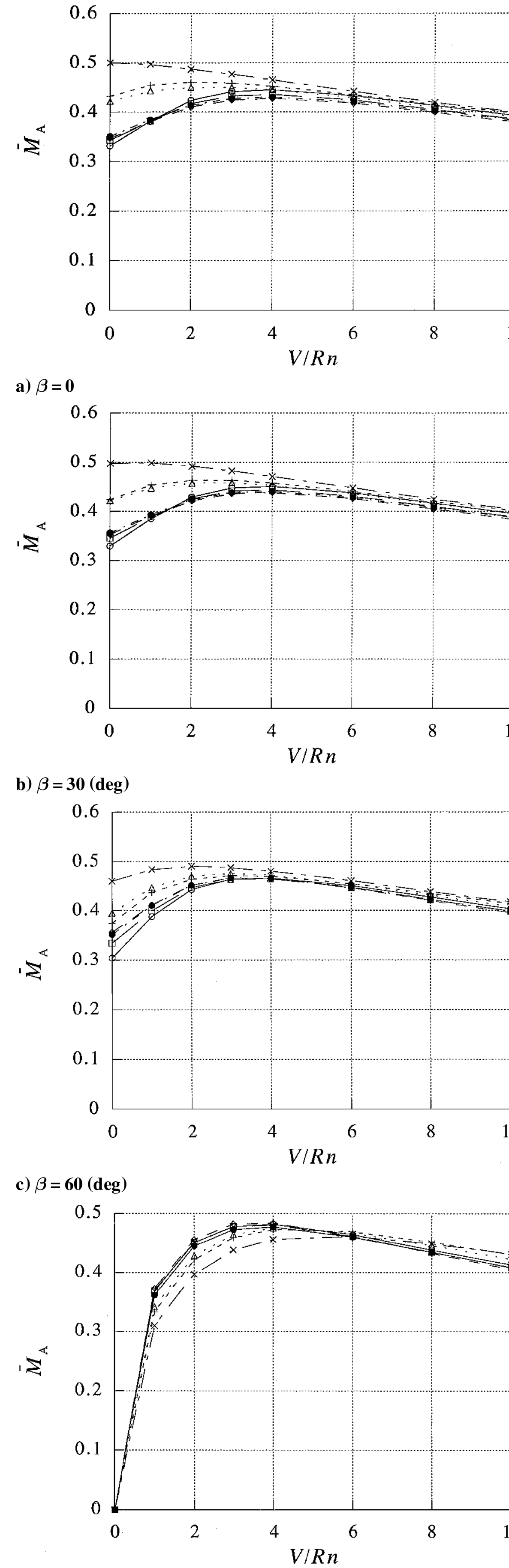

a) $\beta = 0$

b) $\beta = 30$ (deg)

c) $\beta = 60$ (deg)

d) $\beta = 90$ (deg)

Fig. 11 Nondimensional added mass $\bar{M}_A$ of an isolated sheet. (ϕ_{max}, ϕ_{min}): ○, (30,−30); □, (60,−30); ◇, (60,−60); ●, (75,−45); +, (90,−30); △ (90,−60); and ×, (90,−90).

At $V/Rn \leq 2$

In contrast, variations in $\phi_{\max}$, $\phi_{\min}$, and β significantly affect $\bar{M}_A$. The variations in $\hat{M}_A$ are composed of this variation in $\bar{M}_A$ and changes in the vortex-sheet area.

At β = 0, 30, and 60 deg

The value of $\bar{M}_A$ is large when $\phi_{\max}$ or $-\phi_{\min}$ is 90 deg, and is maximum when $\phi_{\max} = -\phi_{\min} = 90$ deg. At $q = 0$ the added mass increases by the interference effect as p approaches two (Fig. 7b), thus indicating that the added mass increases when the two sheets are connected. This is why $\bar{M}_A$ is large when $\phi_{\max}$ or $-\phi_{\min}$ is equal to 90 deg.

At β = 90 deg

The value of $\bar{M}_A$ is large when neither $\phi_{\max}$ or $-\phi_{\max}$ are 90 deg, because the vortex-sheet shape approaches a square when both $\phi_{\max}$ and $\phi_{\min}$ are small.

Conclusions

An approximate method for estimating induced power for flapping flight at any forward velocity has been developed. It uses the added mass of the vortex sheets whose shape is determined by the wing kinematics. In this method the wake geometry is assumed like in methods 1–4, but the present method has the following two advantages. First, it has no discrepancy with either the Rankine–Froude momentum theory for a rotary wing or the momentum theory for a fixed wing. Second, it can be used to determine the effects of most kinematic parameters of flapping wings on the induced power. The effectiveness of the present method was demonstrated by determining the contribution of the following kinematics of flapping wings to decreasing the induced power and increasing the efficiency of flight.

1) During high-speed flight where the inclination of the stroke plane is large, both the amplitude of the flapping angle and the mean flapping angle should be small.

2) During low-speed flight where the inclination of the stroke plane is small, the amplitude of the flapping angle should be large, and the maximum flapping angle is sometimes 90 deg (clap-fling mechanism).

Numerical calculation techniques such as the vortex lattice method and the panel method can estimate induced power without assuming the wake geometry. Compared with these numerical techniques, the present method offers a simpler physical understanding of the effects of kinematic variation on induced power. The computer power required by the present method is also much smaller than that by the numerical methods.

Appendix A: Panels and Vortex Sheets

1) The number $2N$ of panels distributed on a vortex sheet was determined as follows. The value of $i_{\max}$ is equal to that of $j_{\max}$ in all of the calculations in this paper, and so N is given by $i_{\max} j_{\max}$. Values of $\hat{M}_A$ were estimated over a range of N for the cases $\beta = 0$, $\phi_{\max} = -\phi_{\min} = 30$ deg, and $\beta = 0$, $\phi_{\max} = -\phi_{\min} = 90$ deg. The relation between $\hat{M}_A$ and $2N$ is shown in Fig. A1. The values of $\hat{M}_A$ converged sufficiently by $2N = 1250$, and that value was subsequently used in all of the calculations in this paper.

2) The number of sheets *NP* was determined as follows. When the value of w/Rn is smaller, interaction between the sheets increases, and the number of sheets *NP* should be larger. Values of $\hat{M}_A$ were therefore estimated over a range of *NP* for $\beta = 0$, $\phi_{\max} = -\phi_{\min} = 30$ deg, and $w/Rn = 0.5$. The relation between $\hat{M}_A$ and *NP* for this case is shown in Fig. A2. The value of $\hat{M}_A$ is nearly constant over the range, and a value of *NP* equal to 15 was used in all calculations when w/Rn is not smaller than 0.5, that is, all of the calculations except for those for Fig. 4.

Figure A2 also shows the relations between $\hat{M}_A$ and *NP* for the cases for Fig. 4, when $n = 600$, $w/Rn = 0.057$ and $n = 928$, $w/Rn = 0.056$. The values of $\hat{M}_A$ converged sufficiently by $NP = 150$ and 100, respectively, and these values of *NP* were used when the added mass of the vortex sheets was calculated. As just stated, the values of *NP* were determined for Fig. 4 so that the estimated added mass of the vortex sheets is nearly equal to that when the value of *NP* is infinity.

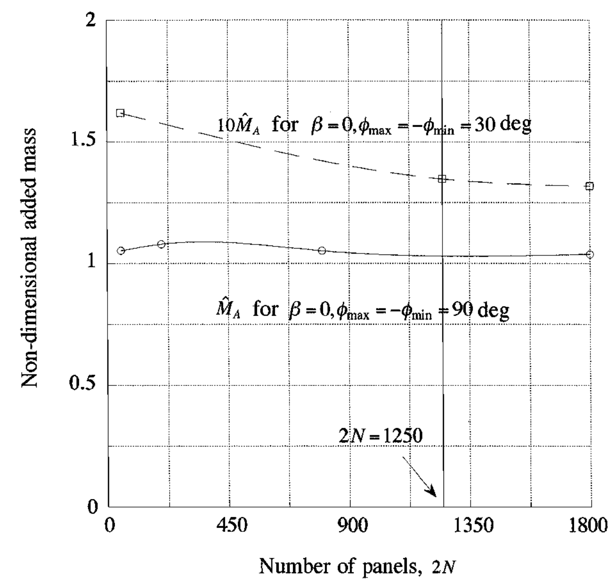

Fig. A1 Relation between the number of panels on the vortex sheet $2N$ and added mass $\hat{M}_A$.

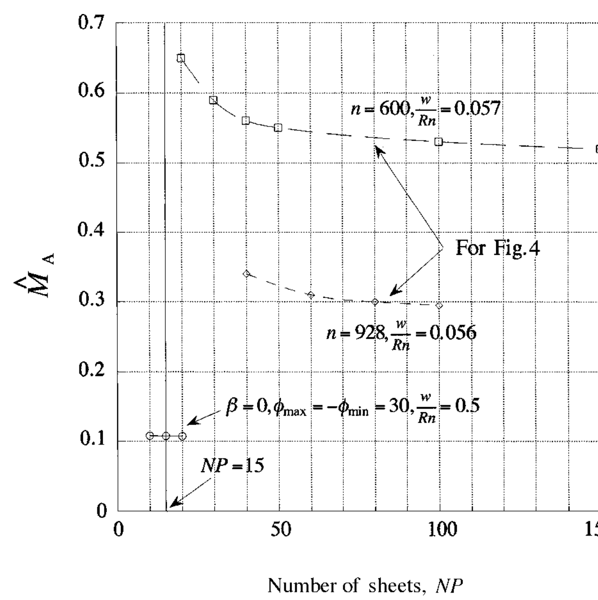

Fig. A2 Relation between the number of sheets *NP* and added mass $\hat{M}_A$.

Appendix B: Kinematic Data

Table B1 shows kinematic data of flights whose induced power were estimated by the present method.

Appendix C: Added Mass of Typical Shapes

Nondimensional added mass $\bar{M}_A = M_A/\rho S^{1.5}$ for an isolated rectangular, elliptical, or isosceles triangular sheet is shown in Fig. C1. The following equation is satisfied for an isolated rectangular or elliptical sheet because of the symmetry of the shape of the sheet:

$$\bar{M}_A(a/b) = \bar{M}_A(b/a) \tag{C1}$$

Therefore, in Fig. C1, we show $\bar{M}_A$ only for $a/b < 1$ for a rectangular or elliptical sheet. Furthermore, the added mass for a rectangular sheet with small a/b is approximately equal to the summation of added mass for a two-dimensional sheet whose width is a:

$$\bar{M}_A(a/b) = (\pi/4)\sqrt{a/b}, \qquad a/b \ll 1 \tag{C2}$$

The maximum $\bar{M}_A$ for a rectangular, elliptical, or isosceles triangular sheet is that for a square, circular, or equilateral triangular sheet, respectively. Furthermore, $\bar{M}_A$ for a square sheet is similar to

Table B1 Wing motions

Insect	M, g	R, mm	V, m/s	ϕ_{max}, deg	ϕ_{min}, deg	β, deg	n, Hz	n_d, Hz	V/Rn
Cranefly[7]	0.0498	17.4	0.376	81.0	−39.0	6	58.0	58.0	0.37
Pigeon[4]	400	325	7.8	86.5	−11.0	45	6.2	6.2	3.9
			9.2	66.0	−15.0	53	6.0	6.0	4.7
			18.0	81.5	−18.5	80	5.6	5.6	9.9
Hawkmoth[16]	1.995	52.1	0.0	72.4	−40.7	23.4	25.4	21.0	0.0
			0.9	69.9	−35.6	23.3	25.6	21.9	0.67
			2.1	74.1	−25.4	37.6	24.8	21.2	1.63
			2.9	70.0	−27.1	44.4	26.1	22.3	2.13
			3.8	73.1	−29.6	52.7	24.8	20.0	2.94
			5.0	73.4	−30.4	56.4	25.0	22.2	3.84
Bumblebee[17]	0.175	13.2	0.0	80.0	−36.0	6	155	155	0.0
			1.0	81.0	−31.0	16	145	145	0.52
			2.5	86.5	−38.5	28	152	152	1.25
			4.5	77.5	−25.5	43	144	144	2.37

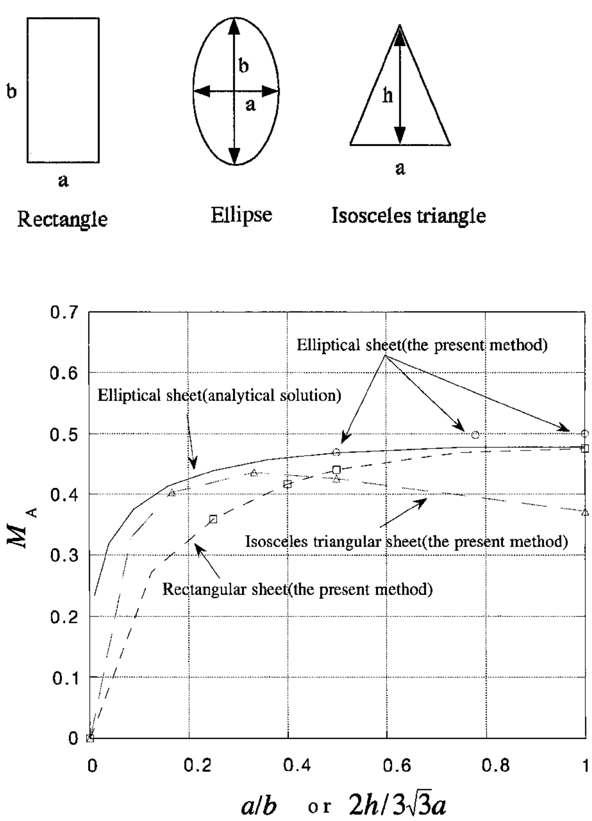

Fig. C1 Nondimensional added masses $\bar{M}_A$ of a rectangular, elliptical, or isosceles triangular sheet.

that for a circular sheet, and both are larger than that for an equilateral triangular sheet.

Acknowledgment

This research was done during a visit to the University of Cambridge by S. S., who was a researcher of the Japan Science and Technology Corp.

References

[1]Philips, P. J., East, R. A., and Pratt, N. H., "An Unsteady Lifting Line Theory of Flapping Wings with Application to the Forward Flight of Birds," *Journal of Fluid Mechanics*, Vol. 112, Nov. 1981, pp. 97–125.

[2]Vest, M. S., and Katz, J., "Unsteady Aerodynamic Model of Flapping Wings," *AIAA Journal*, Vol. 34, No. 7, 1996, pp. 1435–1440.

[3]Hall, K. C., and Hall, S. R., "Minimum Induced Power Requirements for Flapping Flight," *Journal of Fluid Mechanics*, Vol. 323, Sept. 1996, pp. 285–315.

[4]Pennycuick, C. J., "Power Requirements for Horizontal Flight in the Pigeon," *Journal of Experimental Biology*, Vol. 49, No. 3, 1968, pp. 527–555.

[5]Willmott, A. P., and Ellington, C. P., "The Mechanics of Flight in the Hawkmoth *Manduca Sexta*. II. Aerodynamic Consequences of Kinematic and Morphological Version," *Journal of Experimental Biology*, Vol. 200, No. 21, 1997, pp. 2723–2745.

[6]Stepniewski, W. Z., and Keys, C. N., *Rotary-Wing Aerodynamics*, Dover, New York, 1984, pp. 62–65.

[7]Ellington, C. P., "The Aerodynamics of Hovering Insect Flight," *Philosopical Transactions of the Royal Society of London, Series B*, Vol. 305, 1984, pp. 1–181.

[8]Rayner, J. V., "A Vortex Theory of Animal Flight. I. The Vortex Wake of a Hovering Animal," *Journal of Fluid Mechanics*, Vol. 91, Pt. 4, 1979, pp. 697–730.

[9]Rayner, J. V., "A Vortex Theory of Animal Flight. II. The Forward Flight of Birds," *Journal of Fluid Mechanics*, Vol. 91, Pt. 4, 1979, pp. 731–763.

[10]Rayner, J. V., "A New Approach to Animal Flight Mechanics," *Journal of Experimental Biology*, Vol. 80, June 1979, pp. 17–54.

[11]Prandtl, L., and Tietjens, O. G., *Applied Hydro- and Aerodynamics*, Dover, New York, 1934, pp. 185–225.

[12]Katz, J., and Protkin, A., *Low-Speed Aerodynamics from Wing Theory to Panel Methods*, McGraw–Hill, New York, 1991, pp. 421–511.

[13]Sunada, S., Kawachi, K., Watanabe, I., and Azuma, A., "Fundamental Analysis of Three-Dimensional 'Near Fling'," *Journal of Experimental Biology*, Vol. 183, Oct. 1993, pp. 217–248.

[14]Azuma, A., *The Biokinetics of Flying and Swimming*, Springer–Verlag, Tokyo, 1992, p. 221.

[15]Japan Society of Mechanical Engineering, *JSME Mechanical Engineers' Handbook, A5 Fluid Mechanics*, Maruzen, Tokyo, 1984, p. 32 (in Japanese).

[16]Willmott, A. P., and Ellington, C. P., "The Mechanics of Flight in the Hawkmoth *Manduca Sexta*. I. Kinematics of Hovering and Forward Flight," *Journal of Experimental Biology*, Vol. 200, No. 21, 1997, pp. 2705–2722.

[17]Dudley, R., and Ellington, C. P., "Mechanics of Forward Flight in Bumblebees. I. Kinematics and Morphology," *Journal of Experimental Biology*, Vol. 148, Jan. 1990, pp. 19–52.

P. R. Bandyopadhyay
Associate Editor